MRS thermometry calibration at 3T: effects of protein, ionic concentration and magnetic field strength

Babourina-Brooks, Ben; Simpson, Robert; Arvanitis, Theodoros; Machin, Graham ; Peet, Andrew; Davies, Nigel

DOI:
10.1002/nbm.3303

Document Version
Peer reviewed version

Citation for published version (Harvard):
Babourina-Brooks, B, Simpson, R, Arvanitis, T, Machin, G, Peet, A & Davies, N 2015, 'MRS thermometry calibration at 3T: effects of protein, ionic concentration and magnetic field strength', *NMR in biomedicine*, vol. 28, no. 7, pp. 792-800. https://doi.org/10.1002/nbm.3303

MRS Thermometry Calibration at 3T: Effects of protein, Ionic concentration and Magnetic Field Strength

Ben Babourina-Brooks[1,2], Robert Simpson[3], Theodoros N Arvanitis[2,4], Graham Machin[3], Andrew C Peet[1,2], and Nigel Paul Davies[1,5]

[1]School of Cancer Sciences, University of Birmingham, Birmingham, West Midlands, United Kingdom, [2]Birmingham Children's Hospital NHS Foundation Trust, Birmingham, West Midlands, United Kingdom. [3]Temperature Group, National Physical Laboratory, Teddington, Middlesex, UK [4]Institute of Digital Healthcare, WMG, University of Warwick , Coventry, United Kingdom, [5]Imaging & Medical Physics, University Hospitals Birmingham NHS Foundation Trust, Birmingham, West Midlands, United Kingdom

Ben Babourina-Brooks
School of Cancer Sciences
Vincent Drive
University of Birmingham
Birmingham
United Kingdom
B15 2TT

+447505674981
b.brooks@bham.ac.uk

Word Count: 4820

Short Title: MRS Thermometry Calibration: Protein, Ionic and Magnetic field effect.

Sponsors: Birmingham Hospital Charities. CR UK and EPSRC Cancer Imaging Programme at the Children's cancer and Leukaemia Group (CCLG) in association with the MRC and Department of Health (England) (C7809/A10342). NIHR Research Professorship (13-0053) (AP, MW), NIHR/CSO Healthcare Scientists Research Fellowship (ND) and EU Marie curie: International Incoming Fellowship (BB).

Keywords: MRS thermometry, brain temperature, proton resonance frequency, chemical shift, MRI, calibration.

Abbreviations:
National Physical Laboratory (NPL), International Temperature Scale 1990 (ITS-90)
NAA- N-acetylaspartate, bovine serum albumin (BSA), $\Delta_{(H20\text{-}NAA)}$ – Chemical shift difference between H_2O and NAA,
PRF- proton resonance frequency, PRESS - point resolved single voxel spectroscopy,
jMRUI (Java Magnetic Resonance User Interface), Hankel-Lanczos singular value decomposition (HLSVD),
SD- standard deviation, FID- Free induction decay TSPS - **s**odium 3-(trime-thylsilyl)propane-1-sulfonate

Abstract

MRS thermometry has been utilized to measure temperature changes in the brain, which may aid in the diagnosis of brain trauma and tumours. However, the temperature calibration of the technique has been shown to be sensitive to non-temperature based factors, which may provide unique information on the tissue microenvironment if the mechanisms can be further understood. The focus of this study was to investigate the effects of varied protein content on the calibration of the MRS thermometry at 3T, which has not been thoroughly explored in the literature. The effect of ionic concentration and magnetic field strength were also considered. Temperature reference materials were controlled by water circulation and freezing organic fixed-point compounds (diphenyl ether and ethylene carbonate) stable to within 0.2°C. The temperature was measured throughout the scan time with a fluoro-optic probe, uncertainty of 0.16°C. The probe was calibrated at the National Physical Laboratory (NPL) with traceability to the International Temperature Scale 1990 (ITS-90). MRS thermometry measures were based on single voxel spectroscopy chemical shift differences between water and N-acetylaspartate (NAA), $\Delta_{(H20\text{-}NAA),}$ using a Philips Achieva 3T scanner. Six different phantom solutions with varying protein or ionic concentration, simulating potential tissue differences, were investigated within a temperature range of 21-42°C. Results were compared to a similar study performed at 1.5T to observe the effect of field strengths. Temperature calibration curves were plotted to convert $\Delta_{(H20\text{-}NAA)}$ to apparent temperature. The apparent temperature changed by -0.2°C /% of bovine serum albumin (BSA) and a trend of 0.5°C/50mM ionic concentration was observed. Differences in the calibration coefficients for the 10% BSA solution were seen in this study at 3 T compared with a study at 1.5 T. MRS thermometry may be utilized to measure temperature and the tissue microenvironment, which could provide unique unexplored information for brain abnormalities and other pathologies.

Introduction

Brain temperature measures are important for monitoring brain trauma [1], stroke [2], hypothermia [3, 4] and tumours [5], for both thermal treatment [6] and potential diagnosis. However, conventional probes of core temperature, such as tympanic and rectal thermometry, have been shown to be unreliable measures of brain temperature [7, 8]. Invasive methods such as implanted brain temperature sensors may be used for special case neurosurgical patients, however this technique is otherwise difficult to justify clinically. There are a variety of non-invasive temperature-sensitive MR techniques [9]. Whilst most of these are limited to measuring temperature changes, 1H MRS based brain thermometry has the advantage that it can be calibrated to measure actual temperature measures [10]. A potential drawback of ^{1}H MRS for temperature measurement is that tissue microenvironment may affect the measurement and further understanding of this phenomenon is required.

^{1}H MRS thermometry is based on the measurement of the chemical shift difference between the spectral water peak and one or more reference metabolite peaks [10]. The water chemical shift is linearly dependent on temperature, with a coefficient of approximately -0.01ppm/°C, which can be used to provide actual temperature measurements using an appropriate calibration [11-17]. The uncertainty of the technique has been reported to be ± 0.2°C [18] in phantoms using single-voxel MRS at 3T and a set temperature calibration, however it has not been calibrated with demonstrable traceability to the International Temperature Scale 1990 (ITS-90) [19]. While the precision of actual temperature measurements using MRS is dependent on the error in determining the relative water chemical shift, which itself is dependent on the experimental conditions, the main source of error is likely to be due to the accuracy and relevance of the calibration used. Variations in the temperature calibration of the chemical shift have been discussed in the literature, reducing the confidence in accurate thermometry (Table 1). The reported studies were carried out at different magnetic field strengths, using various target materials (e.g., animal and human brain, phantoms) and no demonstrable traceability to the ITS-90 [19]. Tissue or sample composition may affect the calibration due to differences in ionic concentration, fast proton chemical exchange and magnetic susceptibility, all of which may differentially affect the water and reference metabolite chemical shifts. These effects may be dependent on magnetic field strength, providing potential mechanisms by which the temperature calibration of the relative water chemical shift may be field strength dependent.

A recent investigation into the effect of different ionic concentrations, pH levels and a single protein concentration on MRS temperature calibrations, was performed on a 1.5T clinical scanner by Vescovo *et al*. [12]. The study found ionic strength and protein concentration changed the temperature calibration values, compared to a control solution. The equipment for their study was provided by The National Physical Laboratory (NPL), the same equipment has been provided for this study. The NPL is the UK national metrology institute responsible for, among other things, maintaining and disseminating the SI units at the highest level, including the temperature scale. The apparatus, used in this study, was specifically designed to ensure that the sample has a minimal internal temperature gradient and temperature drift throughout the measurement periods.

In this work, we investigate the effect of different protein and ionic concentrations on the temperature calibration at 3T using stable temperature phantoms. These results were then compared with the results of Vescovo *et al* to investigate the

magnetic field strength dependence of the calibration. The comparison was made stronger by the use of the same experimental apparatus, test solutions and large overlap in the data processing methods. .

Table 1: Literature review of temperature calibrations using $\Delta_{(H2O-NAA)}$. Magnetic field strength (B_o), slope of calibration (α), y intercept (β), correlation value (R^2), $\Delta_{(H2O-NAA)}$ chemical shift at 37°C, and change in temperature from this study's neuronal mimic's results are shown.

Methods:

Known temperature phantom references, provided by NPL, were utilized to calibrate MRS thermometry. The temperature fixed-point objects (high purity organic compounds) provided temperature references traceable to ITS-90, stable to < 0.2°C. A water circulating phantom provided a controllable temperature source, stable to within 0.2°C. The two types of phantom consist of two glass spherical compartments, such that the outer sphere fully envelopes the inner one for maximum thermal contact. The one used for the fixed-point organic compounds is shown in Figure 1; the one used for water circulation is similar but has an inlet *and* outlet for the circulating water. The inner sphere (internal diameter, 50 mm) contained the sample solution and the outer sphere (internal diameter, 120 mm) contained the fixed-point temperature reference or circulating water at varying stable reference temperatures. Accurate temperature measurement of the sample was performed with a fluoro-optic thermometer (Luxtron 790, National Instruments UK & Ireland, Newbury, Berkshire, UK), calibrated via a standard platinum resistance thermometer (SPRT) and a stirred temperature controlled water bath, with an estimated uncertainty of 0.16°C (k = 2, 95% confidence).

Figure 1: Spherical glass phantom used for controlled temperature circulation and realising the freezing point of the organic fixed point compounds, the positions of the optical fibre probe, organic compound and sample (e.g. NAA solution) are shown.

Six pH normalised, pH ~ 7, solutions were studied, using NAA (25mM) as the reference metabolite (Table 2) , with four out of the six solutions identical to those used in Vescovo *et al* [12] study to allow investigation of the effect of magnetic field strength on the calibration curve. A control solution and varied NaCl/KCl concentrations, used to approximate the ionic concentration of a neuronal and glial cell [20], facilitated the investigation of the ionic concentration effect on the temperature calibration (Table 2). The control solution and three concentrations of the bovine serum albumin (BSA) protein (5%,10%, 15% w/V) were also used to investigate the effect of protein concentration on the temperature calibration (Table 2). All chemicals were purchased from Sigma-Aldrich (Gillingham, Dorset, UK).

The two glass sphere phantoms were used to provide a stable temperature environment in the outer sphere, which through thermal contact ensures a stable temperature in the sample solution (inner sphere). The fixed-point organic compounds were ethylene carbonate and diphenyl ether, freezing at 35.8°C and 26.3°C, respectively. The procedure used to attain a stable temperature with the frozen organic compounds has been described in detail previously [12]. In short, the organic temperature reference phantoms were heated in a water bath (70°C) for one hour then transferred to a cool water bath (20°C) and left to super-cool (1 hour). The super-cooled organic solution was thermally shocked with dry ice, then left for 30 minutes to ensure the thermally stable semi-solid state was fully achieved. When prepared correctly, the organic materials maintained a stable temperature over the scan time (40 minutes) to within 0.1°C. The water circulation phantom utilizes a water bath of variable temperature (0-100°C), which is connected into and out of the outer sphere of the glass phantom via plastic tubing. Insulation of both the plastic tubing and glass phantom ensured minimal heat loss from the bath to the sample temperature occurred.

MRS temperature measurements were taken within the range of 21-42°C, at 5°C increments (water bath settings of 21, 26, 31, 36, and 41°C) and six MRS measures were taken per temperature point.. After the water bath or fixed point reached specific temperature increments a waiting period of 15 minutes was used to allow for temperature stabilisation within the sample. The sample solution temperature was accurately measured and monitored throughout the MRI scanning with the fluoro-optic thermometer. On average, four temperature points were measured per sample solution, typically three via the water circulation and at least one from the organic fixed-point references. Phantoms were placed in the isocentre of the scanner and there was at least 15 minutes waiting time, to reduce bulk water motion, before the start of scanning.

Phantoms were scanned with a 3T Phillips Achieva (Phillips Medical Inc., Best, The Netherlands). Six single-voxel spectra were recorded at each temperature point using single-voxel point-resolved spectroscopy (PRESS), [TR/TE/NSA = 2000ms/100ms/32, 15x15x15mm^3 volume. 2048 samples], from which the Proton Resonance Frequency (PRF) shift of water relative to NAA, $\Delta_{(H20\text{-}NAA)}$, was measured. The sample volume was placed within the inner sphere, the water and NAA voxel overlap was approximately equidistant from the tip of the temperature probe and the glass edge to minimise bulk susceptibility effects. No water suppression was used during acquisition.

The spectra were processed offline using jMRUI (Java Magnetic Resonance User Interface). The water peak was fitted with the AMARES [21] tool initially to obtain the water PRF. The water peak signal was then artificially suppressed using the Hankel-Lanczos singular value decomposition (HLSVD) method [21, 22] to facilitate accurate modelling of the NAA peak, which was used as the temperature independent reference (Figure 2). Both the water and NAA peak were modelled as single lorentzian lineshapes. The chemical shift was then calculated from the Water-NAA PRF difference, $\Delta_{(H20\text{-}NAA)}$. Mean repeatability measures were calculated using the six $\Delta_{(H20\text{-}NAA)}$ values at each temperature point and then averaged across for the protein and ionic solutions separately.

Figure 2: Example of a HLSVD water suppressed single voxel spectra acquired from the ionic control solution using the diphenyl ether phantom (26.3°C).

The temperature was measured and monitored during the MRS acquisitions using the fluoro-optic probe, with the tip placed immediately adjacent to the MRS sampled volume. The $\Delta_{(H20\text{-}NAA)}$ values were plotted against temperature and linear regression performed on the data. The relationship between the temperature and the water chemical shift relative to NAA, $\Delta_{(H20\text{-}NAA)}$, is given by Equation 1, where T is the temperature and α, β are the coefficients of the slope.

$$T = \alpha\Delta_{(H20\text{-}NAA)} + \beta \qquad (1)$$

This relationship was used to investigate the test solution composition effect on the linear calibration coefficients. The mean α, β were derived from Equation 1 and the measured T and $\Delta_{(H20\text{-}NAA)}$. The variance [$\sigma$] of α, β were based on the goodness of fit measure, R^2. The $\Delta_{(H20\text{-}NAA)}$ at 37°C was also calculated based on the fitted linear coefficients. The $\Delta_{(H20\text{-}NAA)}$ at 37°C for the neuronal cell ($\Delta_{neuronal}$) was used to calculate a temperature difference between the solutions. $\Delta_{neuronal}$ was used in Equation 1 for each temperature calibration curve, providing an apparent temperature value and therefore an apparent temperature difference for each solution relative to the neuronal cell solution, $\Delta T_{neuronal}$. These quantities were used to investigate the magnitude of the differences in apparent temperature values that would be implied by the varying calibration curves dependent upon the test sample characteristics.

Plots of $\Delta_{(H20\text{-}NAA)}$ versus ionic concentration and protein concentration, for three temperature points (31, 36, and 41°C) were made to show the effect of the test solution concentration on the calibration (Figure 4,6). Ionic concentration was calculated by summing the NaCl and KCl concentration within each of the solutions. The mean equilibrated solution temperature measures were subtly different for each solution at the same set bath temperature (21, 26, 31, 36, and 41°C). This was primarily due to bath water temperature variation and small heat loss differences across experiments through the water piping. Therefore, to accurately compare the ionic and protein effects on the $\Delta_{(H20\text{-}NAA)}$ at the same temperature, a linear correction for these small differences was applied. The temperature calibration, Equation 1, was used with the fixed slope coefficients of each solution (Table 2) and fixed temperature values (21, 26, 31, 36 or 41°C) to calculate the water PRF relative to NAA at the fixed temperature values. Error bars were calculated based on the standard error from the six MRS measures at each temperature point.

Plots of $\Delta_{(H20\text{-}NAA)}$ against temperature for this study compared with results from the literature were created. These plots were produced by extrapolating results in each study to allow a convenient visual comparison of the temperature calibration curves, (shown in Figure 7). Five specific chemical shift values (2.63, 2.64, 2.65, 2.66, 2.67 ppm) were used in conjunction with calibration coefficients, α, β, for each study to predict the probe temperature. Error bars calculated based on the residual fitting error and attributed to the temperature measure, where possible. These values were plotted to determine the difference between the calibration curves.

Linear regression analysis was used to compare temperature calibration curves, using R^2 for goodness of fit, and $p<0.05$ was used as the threshold for significance of pearson correlation measures.

Results

$\Delta_{(H20\text{-}NAA)}$ measurements of the six pH normalized solutions at a range of temperatures were made. Plots of $\Delta_{(H20\text{-}NAA)}$ versus temperature were constructed and the differences between solutions investigated (Table 2, Figure 3 and 4). Fits of the water and NAA peak produced residuals within the noise and the spectral linewidths of the NAA metabolite peak were less than 3 Hz. Narrow linewidths and good modelling of the peaks ensured the HLSVD routine works well at removing the water signal and reproducible $\Delta_{(H20\text{-}NAA)}$ values could be obtained. The meanrepeatability of the $\Delta_{(H20\text{-}NAA)}$ (apparent temperature) measurements were 0.00651 ppm (0.65°C) and 0.00554(0.5°C) for the protein and ionic solutions, respectively. Test solution temperature measurements were reproducible with a standard deviation of ~ $\pm$0.02° C and ~ $\pm$0.05 °C for the fixed point and water circulation, respectively, during the MRS measurements.

Table 2: Temperature calibration results from the six solutions and the Vescovo *et al* study. Slope of calibration (α), y intercept (β), correlation value (R^2), $\Delta_{(H20\text{-}NAA)}$ at 37°C, and the change in apparent temperature from this study's neuronal solution.

There were strong linear correlations between the $\Delta_{(H20\text{-}NAA)}$ of the six solutions and temperature with high correlation coefficients, $R^2>0.99$, (Table 2). The α, β and $\Delta_{(H20\text{-}NAA)}$ at 37°C were sensitive to the concentration of the solution.

Ionic concentration solutions

There were $\Delta_{(H20\text{-}NAA)}$ differences between the three ionic concentration controlled solutions at constant temperature, as shown in Figure 3. There was good reproducibility of the measurements, as shown by the small standard deviations, and there is reasonable evidence of a linear trend of $\Delta_{(H20\text{-}NAA)}$ with ionic concentration. Small standard deviation of the

measurements and high R^2 values were found for all three ionic solutions. Table 2 shows that there is a trend of decreasing $\Delta_{(H20\text{-}NAA)}$, α, β and apparent temperature with increasing ionic concentration, p=0.09. Figure 3 illustrates this result by the data points for the glial ionic concentration solution being shifted to the left along the x-axis compared with the ionic control. A plot of $\Delta_{(H20\text{-}NAA)}$ versus ionic concentration for each temperature point shows this result clearly, Figure 4. Assuming the ionic concentration effect on the $\Delta_{(H20\text{-}NAA)}$ is linear, then the average slope across temperatures is ~ -7.5x10^{-5}ppm/mM, (~0.0075°C/mM).

Figure 3: Temperature versus $\Delta_{(H20\text{-}NAA)}$ plots of the ionic control, neuronal ionic concentration and glial ionic concentration solutions. The trendline shown is based on the ionic control solution.

Figure 4: Plots of $\Delta_{(H20\text{-}NAA)}$ versus ionic concentration at different set temperatures (26, 31, 36, 41°c). Trend-line linear analysis results are also shown.

Protein concentration solutions

The slope coefficients, $\Delta_{(H20\text{-}NAA)}$ at 37°C and ΔT varied across the protein solutions (Table 2). A statistically significant trend of increasing chemical shift, increasing α, β and apparent temperature, with increased protein concentration was found, $p<0.05$. The results for the ionic control and three protein solutions are plotted in Figure 5, showing large differences between the calibrations. This is highlighted further in the $\Delta_{(H20\text{-}NAA)}$ versus protein concentration plot (Figure 6). There were no significant differences between the slopes of $\Delta_{(H20\text{-}NAA)}$ versus protein concentration for the three different temperatures. The mean slope measuring the protein effect on the $\Delta_{(H20\text{-}NAA)}$ was found to be ~ 0.002 ppm/protein % (~-0.2°C/protein %).

Figure 5: Temperature versus $\Delta_{(H20\text{-}NAA)}$ plots of the ionic control, 5%, 10% and 15% protein concentration solutions. The trendlines shown are based on the ionic control and the 15% protein concentration solutions.

Figure 6: Plots of $\Delta_{(H20\text{-}NAA)}$ versus protein content at different set temperatures (31, 36, 41°c). Trend-line linear analysis results are also shown.

Comparison of 1.5T against 3T

The results for the three ionic solutions and BSA 10% solution from this study (3T) were plotted with the results of the corresponding solutions from the Vescovo *et al* (1.5T) study, Figure 7. Another study, Corbett *et al* (4.7T), using BSA 10% to investigate protein concentration effects on the temperature calibration curve was also observed, but not included in the plot as the solution and analysis protocol were different to the other studies. The ionic control and glial ionic concentration mimics compared extremely well across the studies using different magnetic field strengths. The neuronal solution did not compare as well, however based on this study's standard error there would be a large overlap between the results from each study. The temperature curve for the BSA 10% solution was different in this study compared with the Vescovo *et al* (~1.5°C) and Corbett *et al* studies. (~3°C). There would not be a large overlap of these curves based on the standard error values measured in this study.

Figure 7: Simulated temperature calibration curves based on set chemical shifts and calculated probe temperatures using calibration coefficents. Ionic (a), glial (b), neuronal (c) and BSA 10% (d), from the results of the study here (BBB) and Vescovo *et al* (1.5T, labelled V) are shown.

Discussion:

The $\Delta_{(H2O - NAA)}$ was measured for six different solutions to determine the effects of ionic concentration and protein-mediated fast-exchange on the water PRF - temperature calibration curve at 3T. As expected, $\Delta_{(H20\text{-}NAA)}$ strongly correlated with temperature with small residuals and reproducible results. The water PRF is affected by electron shielding, which is modulated by changes in temperature, since this increases or decreases the mean hydrogen bond length [23]. However, changes to the electron shielding, through factors other than temperature, would affect the temperature calibration curve, and hence reduce the accuracy of MRS thermometry if such affects are not accounted for. Evaluating the sensitivity of the calibration curve to non-temperature related factors is not only important for improving the accuracy and reliability of *in vivo* MRS thermometry, but may also allow novel characterisation of the tissue microenvironment. In this study, the sensitivity of the calibration curves to ionic and protein concentration was assessed *in vitro* (Table 2). These factors vary between tissue types and in disease processes, emphasising the importance of taking this into account when interpreting *in-vivo* MRS thermometry. Additional factors relevant to *in-vivo* measurements, such as tissue microstructure, heterogeneity anisotropy and orientation with the magnetic field are also likely to influence the water PRF – temperature calibration. Combinations of these factors may, at least in part, explain the variation in calibration coefficients obtained in this and previous *in vivo* and *in vitro* studies, as listed in Table 1; though lack of traceability to a defined temperature reference may also have contributed to the observed variation. However, the influence of these factors on the calibration curve, and whether this influence depends on magnetic field strength, have not been systematically investigated. The

results of this study were compared to a previous study conducted with almost identical test solutions and temperature calibration apparatus at 1.5T. Therefore, this study contributes to the existing knowledge base by allowing an assessment of the effect of magnetic field strength on the calibration curves, as well as providing a detailed investigation of the dependence on the fast-exchange effect at multiple protein concentrations.

Ionic effect

Ionic concentration changes lengthen or shorten the mean hydrogen bond length through electrostatic effects [23, 24]. However, whether this effect is measurable by MRS thermometry has been questioned. There have been reports that the ionic concentration does [3, 13] and does not affect the temperature calibration curve, measured via MRS [12]. The results in this study show a trend for a decrease in α, β (Table 2) and $\Delta_{(H20\text{-}NAA)}$ (Figure 3, 4) with increasing ionic concentration. A stronger correlation ($p<0.01$) was found by Vescovo *et al*, which may be due to a larger ionic concentration range (0-400mM) measured and the additional solutions investigated (three in this study versus five in Vescovo *et al*), increasing the significance of the result. Interestingly, the effect of ionic concentration found on the $\Delta_{(H20\text{-}NAA)}$ at a fixed temperature by their study, with a slope of $-9.0\text{x}10^{-5}$ppm/mM, is similar to the results of this study, with a slope of $-7.5\text{x}10^{-5}$ppm/mM (Figure 4). Both results suggest the effect of a change in ionic concentration on the apparent temperature would be ~ -0.008 °C/mM. A study using Na^{23} imaging reported ionic differences of ~ 8mM between basal ganglia and white matter, ~ 38mM between healthy brain and astrocytoma brain tumours [25]. This would imply apparent temperature differences of approximately 0.06°C and 0.30°C for basal ganglia versus white matter and healthy versus tumour tissue respectively, based solely on ionic concentration differences if the same calibration were used. Therefore, the effect of ionic concentration variations on measurements of the apparent temperature is likely to be small for healthy brain, but may be considerable for apparent temperature measurements in tumours and other pathologies.

Protein-mediated fast-exchange effect

Solutions with varying protein content were used to investigate the effects of fast chemical exchange on the water PRF. It has been shown that increased protein content increases the $\Delta_{(H20\text{-}NAA)}$, demonstrated in Figures 5 and 6. Assuming the protein effect is linear, the graphs show similar slopes at the set temperatures, 31°C, 36°C and 41°C. The α and β changes with protein content were found to be linear, ($R^2>0.99$), which suggests the protein effect on the $\Delta_{(H20\text{-}NAA)}$ is approximately linear within the range of concentrations tested.

A number of MRS thermometry studies have investigated the effect of protein concentration on the calibration curve [16], shown in Table 1. The α and β values found in this study are comparable to the Vescovo *et al* results but not the Corbett *et al* results, which may be partly due to the high ionic concentration (150mM) in their protein solutions compared to the solutions reported here (ionic concentration of 0 mM) and differences in postprocessing methods. The $\Delta_{(H20\text{-}NAA)}$ change, at a set temperature, with protein concentration was investigated for each experiment with the results from this study shown in Figure 6. The protein effect on the $\Delta_{(H20\text{-}NAA)}$ independent of temperature was found to be approximately 0.002

ppm/protein%, which compares well to that found by Vescovo *et al* of 0.0025 ppm/protein%, although Vescovo's result was only based on two data points compared to four in this study. Protein concentrations in healthy brain can vary by up to 5% [26]. According to the results of this and Vescovo's study such a variation in protein concentration would correspond to a difference in the apparent temperature of approximately 1°C if the same calibration were used. However, fast exchange effects are not based solely on protein concentration as tissue microstructure, anisotropy and water content are also potentially important factors and should be considered for in-vivo measurements. Grey matter and white matter have similar protein content (~ 1% difference) but have different water content [27], 70% versus 80%, potentially leading to $\Delta_{(H20\text{-}NAA)}$ differences. MRS thermometry measures may also have to consider micro-magnetic susceptibility affects based on orientation with the field, which will vary with protein content and tissue structure [28]. Therefore, caution needs to be taken when assessing brain temperature measurements of differing tissues using MRS thermometry.

Field Strength

Although magnetic field strength does not directly affect the relative water PRF, there are possible indirect effects of the magnetic field strength on the temperature calibration curve related to the factors investigated in this work. These effects have been suspected to contribute to variations in the calibration coefficients reported in the literature by studies using a wide range of magnetic field strengths. Effects of water moving through a static magnetic field [29], salt mobilization [30] and proton relaxation rate [31] all disrupt the hydrogen bonding and increase with field strength. Magnetic susceptibility effects also increase with magnetic field strength and may affect the relative water PRF through microscopic differences between the environments of the water and reference molecules [28].

The temperature calibration curves for the ionic solutions showed small differences between this study at 3T and that of Vescovo *et al* at 1.5T, although this does not rule out significant effects at higher field strengths or in more complex microenvironments. A MRSI based MR thermometry study investigating field strength effects, 1.5T versus 3T, also showed no magnetic field affects were observed on the temperature calibration curve using an ionic concentration solution of 56mM [32]. In contrast, the calibration curves with varying protein concentration presented here, did show different mean results compared with those of Vescovo *et al* at 1.5T, (see Figure 7 d). The BSA solution in Vescovo *et al*'s study contained a higher concentration of phosphate buffer, which may have influenced the comparison. However, in their work, no significant differences were found between two ionic solutions with differing phosphate buffer concentrations (20mM versus 10mM), which suggests that this cannot account for the differences in the protein calibration curves found at 3T, compared with 1.5T . In Corbett *et al*'s study at 4.7T, the solution contained ionic salts (150mM KCl), which based on our glial cell results, could actually explain an increase in apparent temperature of ~1.5°C, at a given specific value of $\Delta_{(H20\text{-}NAA)}$. However, the combination of ionic and protein concentration effects on the temperature calibration curve has yet to be investigated and therefore may not yield a linear response, investigating this is future work. Therefore, taking these differences into account, a magnetic field increase across studies from 1.5T to 3T and 4.7T seems to reduce the $\Delta_{(H20\text{-}NAA)}$ at a given temperature. This implies that magnetic susceptibility effects may be a contributing factor to the observation [28]. Measurements were taken using different scanners with slightly different parameters, likely differences

in field homogeneity and small differences in post-processing methods (first order phase correction, residual baseline treatment, etc), potentially resulting in a systematic bias that may have contributed to some of the differences observed between the studies. However, this is a plausible finding, which should be taken into account, when comparing temperature measurements at different field strengths using MRS thermometry.

Conclusion

MRS thermometry calibration curves were dependent on protein content and sensitive to ionic strength when measured on a 3T scanner. This is an important finding in the light of known protein and tissue structure differences in healthy and diseased human brain, with specific implications for the assessment of MRS temperature measures in different brain tumour types. The comparison between MRS temperature calibrations at 3T and 1.5T, using consistent experimental apparatus, showed that the effect of protein concentration may vary with magnetic field strength, while the ionic effect may not. These findings warrant further investigation into the dependence of protein contents and microstructure on MRS temperature calibrations in more tissue-like materials. The $\Delta_{(H20\text{-}NAA)}$ value is not only a probe for temperature measures but a measure of tissue microenvironment as well.

Acknowledgements

We would like to thank Andrew Levick for his contribution to the early part of this work.
We would also like to thank Jane Crouch for co-ordinating the study and Rachel Grazier for data management. We thank the staff at the Birmingham Children's Hospital and NIHR for use of the imaging facilities. This work was partially funded by the Birmingham Children's hospital Charities research fund and an EU Marie Curie International Incoming fellowship.

References:

1. Soukup J, Zauner A, Doppenberg EM, Menzel M, Gilman C, Young HF, and Bullock R. *The importance of brain temperature in patients after severe head injury; relationship to intracranial pressure, cerebral perfusion pressure, cerebral blood flow, and outcome.* Neurotrauma, 2002. **19**: p. 559-571.
2. Corbett R J T, Purdy P D, Laptook A R, Chaney C, and Garcia D. *Non-invasive measurement of brain temperature after stroke.* Am. J. Neuroradiol, 1999. **20**: p. 1851-1857.
3. Corbett R, Laptook A, and Weatherall P. *Non-invasive measurements of human brain temperature using volume-localised proton magnetic resonance spectroscopy. .* J. Cereb Blood Flow Metab., 1997. **17**: p. 363-369.

4. Weis J, Covaciu L, Rubertsson S, Allers M, Lunderquist A, and Ahlstrom H. *Non-invasive monitoring of brain temperature during mild hypothermia.* Magn. Reson. Imaging., 2009. **27**: p. 923-932.
5. Babourina-Brooks B, Wilson M, Arvanitis TN, Peet AC, and Davies NP. *MRS Thermometry of childhood brain tumours: Temperature changes and the tumour environment.* NMR Biomed, 2014. **In press**.
6. Sapareto SA and Dewey WC, *Thermal dose determination in cancer therapy.* Int J Radiat Oncol Biol Phys, 1984. **10**(6): p. 787-800.
7. Kirk D, Rainey R, Vail A, and Childs C. *Infra-red thermometry in neuro-critical care: how reliable are tympanum and temperal artery measurements for predicting brain temperature?* Crit. Care, 2009. **13**: p. R81.
8. Childs C and Machin G. *Reliability issues in human brain temperature measurement.* Crit. Care, 2009. **13**: p. R106.
9. Reike V and Pauly KB. *MR Thermometry.* J Magn Reson 2008. **27**(2): p. 376-390.
10. Cady E B, D'Souza P C, Penrice J, and Lorek A. *The estimation of local brain temperature by in vivo 1H magnetic resonance spectroscopy.* Magn. Reson. Med., 1995. **33**: p. 862-867.
11. Hindman J C. *Proton resonance shift of water in the gas and liquid states.* J. Chem. Phys., 1966. **44**: p. 4582-4592.
12. Vescovo E, Levick A, Childs C, Machin G, Zhao S, and Williams S R. *High-precision calibration of MRS thermometry using validated temperature standards: effects of ionic strength and protein content on the calibration.* NMR Biomed, 2013. **26**(2): p. 213-223.
13. Zhu M, Bashir A, Ackerman J, and Yablonskiy D A. *Improved calibration technique for in vivo proton MRS thermometry for brain temperature measurement.* Magn. Reson. Med., 2008. **60**: p. 536-541.
14. Kuroda K, Takei N, Mulkern RV, Oshio K, Nakai T, Okada T, Matsumura A, Yanaka K, Hynynen K, and Jolesz FA. *Feasability of internally referenced brain temperature imaging with a metabolite signal.* Magn. Reson. Med., 2003. **2**: p. 17-22.
15. Cady E B, Penrice J, and Robertson N J. *Improved reproducibility of MRS regional brain thermometry by 'amplitude-weighted combination'.* NMR Biomed, 2010. **24**: p. 865-872.
16. Corbett R J T, Laptook A R, Tollefsbol G, and Kim B. *Validation of a noninvasive method to measure brain temperature in vivo using 1H NMR spectroscopy.* J. Neurochem., 1995. **64**: p. 1224-1230.
17. Covaciu L, Rubertsson S, Ortiz-Nieto F, Ahlstrom H, and Weis J. *Human Brain MR spectroscopy thermometry Using Metabolite Aqueous-Solution Calibrations.* J Magn Reson, 2010. **31**: p. 807-814.
18. Childs C, Hiltunnen Y, Vidyasagar R, and Kaupinnen R. *Determination of regional brain temperature using proton magnetic resonance spectroscopy to assess brain-body temperature differences in healthy human subjects.* Magn. Reson. Med., 2007. **57**: p. 59-66.
19. Preston-Thomas, H. *The international temperature scale of 1990 (ITS-90).* Metrologia, 1990. **27**(1): p. 3-10.
20. Erecinska M and Silver IA. *Ions and energy in mammalian brain.* Prog. Neurobiol., 1994(43): p. 37-71.
21. Vanhamme L. *Improved method for accurate and efficient quantification of MRS data with use of prior knowledge.* J Magn Res, 1997. **129**: p. 35-43.
22. laudadio T, Mastronardi N, Vanhamme L, Van Hecke P, and Van Huffel S. *Improved Lanczos algorithms for blackbox MRS data quantitation.* NMR Biomed, 2002. **57**: p. 292-297.
23. Muller N and Reiter R C. *Temperature dependence of chemical shifts of protons in hydrogen bonds.* J. Chem. Phys., 1965. **42**: p. 3265-3269.
24. Sare E J, Moynihan C T, and Angell C A. *Proton magnetic resonance chemical shifts and the hydrogen bond in concentrated aqueous electrolyte solutions.* J. Chem. Phys., 1973. **77**: p. 1869-1876.
25. Ouwerkerk R, Jacobs M A, Macura K J, Wolff A C, Stearns V, Mezban S D, Khouri N F, Bluemke D A, and Bottomley P A. *Tissue sodium concentration in human brain tumors as measured with 23Na MR imaging.* Radiology, 2003. **12**(2): p. 529-537.
26. Banay-schwartz M, Kenessey A, DeGuzman T, Lajtha A, and Palkovits M. *Protein-content of various regions of rat-brain and adult and aging human brain.* Age, 1992. **15**: p. 51-54.
27. Tofts P. *Quantitative MRI of the brain: measuring changes caused by disease.* Wiley:Chicester, 2003: p. 93-97.
28. Luo J, He X, d'Avignon A, Ackerman J J, and Yablonskiy D A. *Protein-induced water 1H MR frequency shifts: Contributions from magnetic susceptibility and exchange effects.* J Magn Res, 2010. **202**: p. 102-108.
29. Chang KT and Weng CI. *An investigation into the structure of aqueous NaCl electrolyte solutions under magnetic fields.* Comput. Mat. Sci, 2008. **43**: p. 1048-1055.
30. Szczes A, Chibowski E, Holysz, and Rafalski P. *Effects of static magnetic field on water at kinetic condition.* Chem. Eng. Procss, 2011. **50**: p. 124-127.

31. Bryant RG, Mendelson DA, and Lester CC. *The magnetic field dependence of proton spin relaxation in tissues.* Magn. Reson. Med., 1991. **21**(1): p. 117-126.
32. Thrippleton MJ, Parikh J, Harris BA, Hammer SJ, Semple SIK, Andrews PJD, Wardlaw JM, and Marshall I. *Reliability of MRSI brain temperature mapping at 1.5 and 3T.* NMR Biomed, 2014. **27**(2): p. 183-190.

Calibration	$T = \alpha\Delta+\beta$				
	B_o (T)	α	β	R^2	Δ at 37°C
Pig brain *in vivo (*Weis *et al*. [4])	1.5	-82.70 (7.49)	258.67(20.17)	0.797	2.6804
Rat brain *in vivo* (Zhu *et al*. [13])	11.7	-103.8(1.9)	313.7(5.1)	0.990	2.6657
Rabbit brain *in vivo* (Kuroda *et al*. [14])	3	-103	310.4	0.932	2.6544
Dog brain *in vivo* (Corbett *et al*. [2])	1.5	-82.33(6.58)	255.94(1.30)	0.710	2.6593
Piglet brain *in vivo* (Cady *et al*. [10])	7	-94.0(3.7)	286.9(10.1)		2.6585
Piglet brain *in vivo* (Cady *et al*. [15])	3	-92.2	282	0.97	
Water, NAA (20mM), Ion and buffer concentrations not given (Kuroda *et al*. [14])	3	-103	313	1.00	2.6796
Water, NAA (10mM), Ion and buffer concentrations not given. Ph=7.1. (Cady *et al*. [10])	7	-97.6(0.6)	293.1 (1.6)		2.6240
Water, NAA (20mM), KCl (150mM), $MgCl_2$ (1.5mM), 6.6 or 9.9mM lactate, pH 7.1 (Corbett *et al*. [16])	4.7	-97.26(0.59)	293.28(0.37)	0.998	2.6350
As above but BSA 8% (Corbett *et al*. [16])	4.7	-97.82(0.57)	295.24(0.34)	0.999	2.6400
As above but BSA 10% (Corbett *et al*. [16])	4.7	-98.38(0.53)	296.42(0.30)	0.999	2.6369
Water, NAA(50mM), pH buffer TSPS(3mM, pH 7.2), K_2HPO_4 (72mM), KH_2PO_4 (28mM), sodium for-mate (NaFor HCOONa, 200mM), NaN_3 (1 g/L) (Covaciu et al [17])	1.5	-97.13 (0.73)	296.07 (2.06)	0.999	2.667
Ionic control: Water, NAA (25mM), phosphate buffer (20mM, pH ~7) (Vescovo *et al*. [12])	1.5	-99.7(0.8)	301.60(2.2)	0.999	2.6540
Neuronal cell: Water, NAA (25mM), KCl (83mM), NaCl (26mM), phosphate buffer (10mM, pH ~7) (Vescovo *et al*. [12])	1.5	-100.85(1.50)	303.56(4.0)	0.999	2.6431
Glial cell: Water, NAA (25mM), KCl (136mM), NaCl (20mM), phosphate buffer (10mM, pH ~7) (Vescovo *et al*. [12])	1.5	-100.60(0.5)	302.30(1.3)	0.999	2.6372
BSA 10%: Water, NAA (25mM), phosphate buffer (20mM, pH ~7) (Vescovo *et al*.[12])	1.5	-105.81	320.25		2.6770

Table 1: Literature review of temperature calibrations using NAA as a water chemical shift reference. Magnetic field strength (B_o), slope of calibration (α), y intercept (β), correlation value (R^2) and $\Delta_{(H2O\text{-}NAA)}$ chemical shift at 37°C are shown. Where available, variation based on the error in the fit are shown in the parentheses.

Phantom solution	$T = \alpha\Delta_{(H20\text{-}NAA)} + \beta$ α	β	R^2	$\Delta_{(H20\text{-}NAA)}$ ppm at 37°C	$\Delta T_{neuronal}$
Ionic control (water, NAA 25mM, phosphate buffer 10mM)	-106.20 (2.33)	318.65 (3.81)	0.992	2.652 (0.006)	-0.30 (0.64)
Neuronal cell ionic concentration (KCL83mM, NaCl 26mM, NAA 25mM, phosphate buffer 10mM)	-105.41 (2.15)	316.26 (3.53)	0.993	2.649 (0.006)	0.00 (0.64)
Glial cell ionic concentration (KCL 136mM, NaCl 20mM, NAA 25mM, phosphate buffer 10mM)	-101.72 (1.59)	305.16 (2.61)	0.997	2.636 (0.004)	0.90 (0.41)
Protein 5% (water, NAA 25mM, phosphate buffer 10mM, BSA 5% W/V)	-94.65 (1.40)	289.13 (2.31)	0.999	2.664 (0.003)	-1.37 (0.30)
Protein 10% (As above, BSA 10% W/V)	-104.13 (1.54)	314.57 (2.55)	0.998	2.666 (0.004)	-1.70 (0.37)
Protein 15% (As above, BSA 15% W/V)	-113.20 (1.56)	340.82 (2.57)	0.999	2.684 (0.003)	-3.92 (0.35)
Vescovo – ionic control (water, NAA 25mM, phosphate buffer 20mM)	-99.70(0.80)	301.60(2.2)	0.999	2.654 (0.003)	-0.50 (0.26)
Vescovo - Neuronal cell (KCL83mM, NaCl 26mM, NAA 25mM, phosphate buffer 10mM	-100.85(1.50)	303.56(4.0)	0.999	2.643 (0.003)	0.65 (0.27)
Vescovo- Glial cell KCL 136mM, NaCl 20mM, NAA 25mM, phosphate buffer 10mM	-100.60(0.50)	302.30(1.30)	0.999	2.637 (0.003)	1.27 (0.27)
Vescovo - BSA 10% (25mM NAA, 20mM phosphate buffer)	-105.81	320.25		2.677	-2.92

Table 2: Temperature calibration results from the six solutions and the Vescovo *et al*. study. Slope of calibration (α), y intercept (β), correlation value (R^2), $\Delta_{(H20\text{-}NAA)}$ chemical shift at 37°C, and the change in apparent temperature from this study's neuronal solution. Variation based on the error of the fit are shown in the parentheses.

Figure 1: Spherical glass phantom used for controlled temperature circulation and realising the freezing point of the organic fixed point compounds, the positions of the optical fibre probe, organic compound and sample (e.g. NAA solution) are shown.

Figure 2: Example of a HLSVD water suppressed single voxel spectrum acquired from the ionic control solution using the diphenyl ether phantom (26.3°C).

Figure 3: Temperature versus $\Delta_{(H20\text{-}NAA)}$ plots of the ionic control, neuronal ionic concentration and glial ionic concentration solutions. The trendline shown is based on the ionic control solution.

Figure 4: Plots of $\Delta_{(H20\text{-}NAA)}$ versus ionic concentration at different set temperatures (26, 31, 36, 41°c). Trend-line linear analysis results are also shown.

Figure 5: Temperature versus $\Delta_{(H20\text{-}NAA)}$ plots of the ionic control, 5%, 10% and 15% protein concentration solutions. The trendlines shown are based on the ionic control and the 15% protein concentration solutions.

Figure 6: Plots of $\Delta_{(H20\text{-}NAA)}$ versus protein content at different set temperatures (31, 36, 41°c). Trend-line linear analysis results are also shown.

Figure 7: Simulated temperature calibration curves based on set chemical shifts and calculated probe temperatures using calibration coefficients. Ionic (a), glial (b), neuronal (c) and BSA 10% (d), from the results of the study here (BBB) and Vescovo *et al* (1.5T, labelled V) are shown.

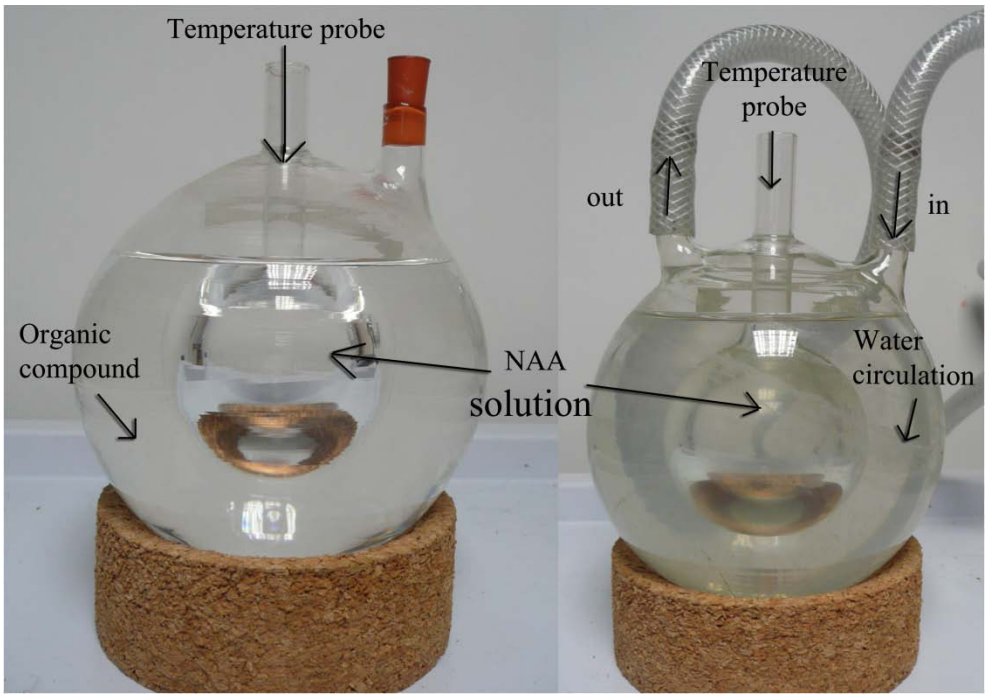

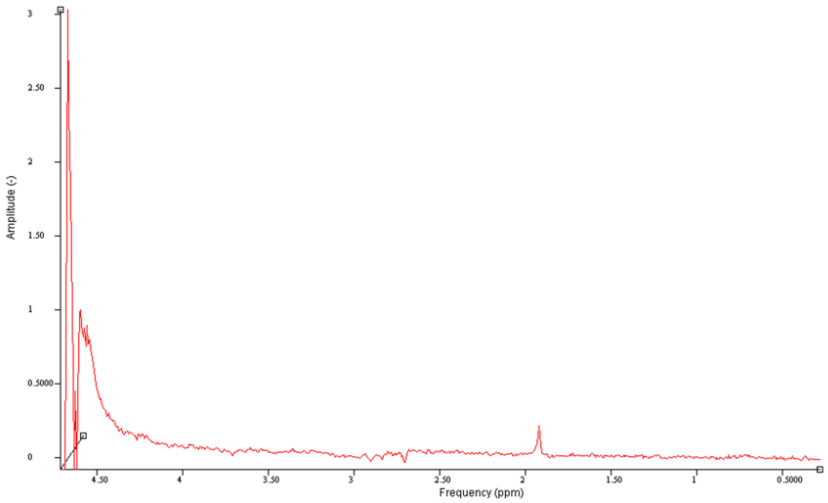
Amplitude (-)
Frequency (ppm)

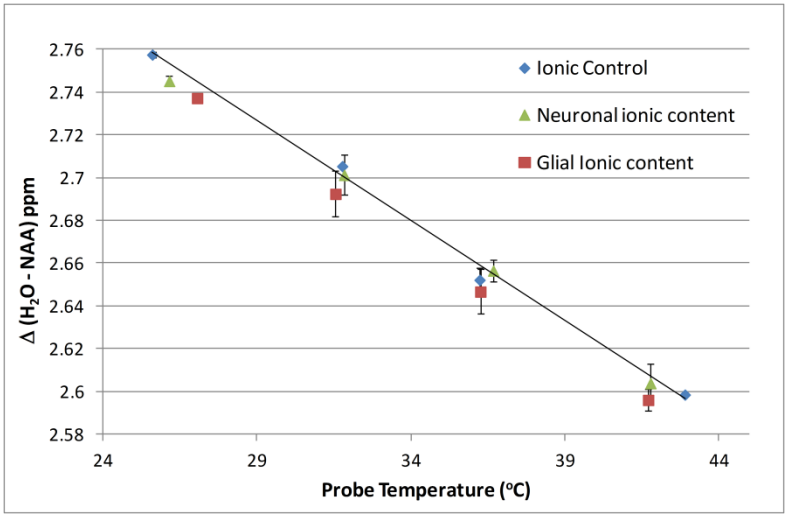
Ionic Control
Neuronal ionic content
Glial Ionic content
Δ (H2O - NAA) ppm
Probe Temperature (°C)

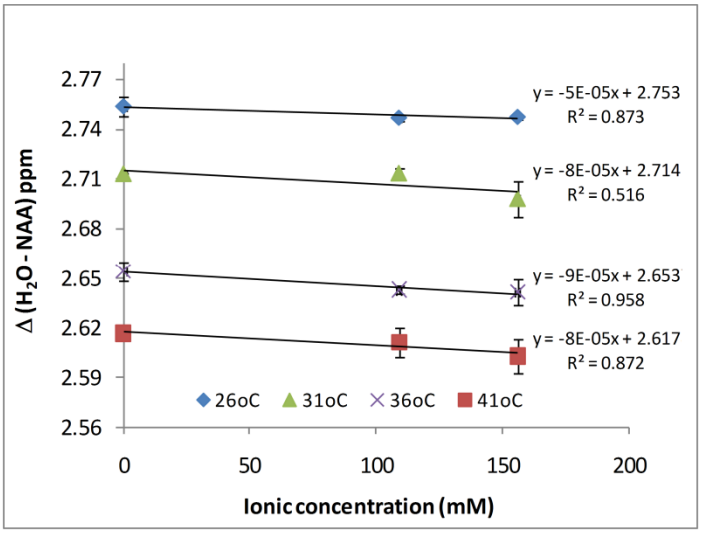
y = -5E-05x + 2.753
R² = 0.873
y = -8E-05x + 2.714
R² = 0.516
y = -9E-05x + 2.653
R² = 0.958
y = -8E-05x + 2.617
R² = 0.872
26oC
31oC
36oC
41oC
Δ (H2O - NAA) ppm
Ionic concentration (mM)

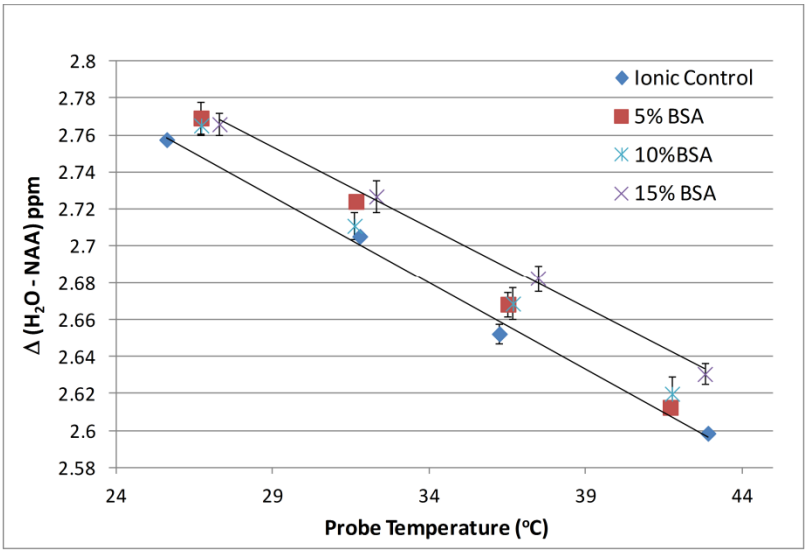
Ionic Control
5% BSA
10%BSA
15% BSA
Δ (H2O - NAA) ppm
Probe Temperature (ºC)

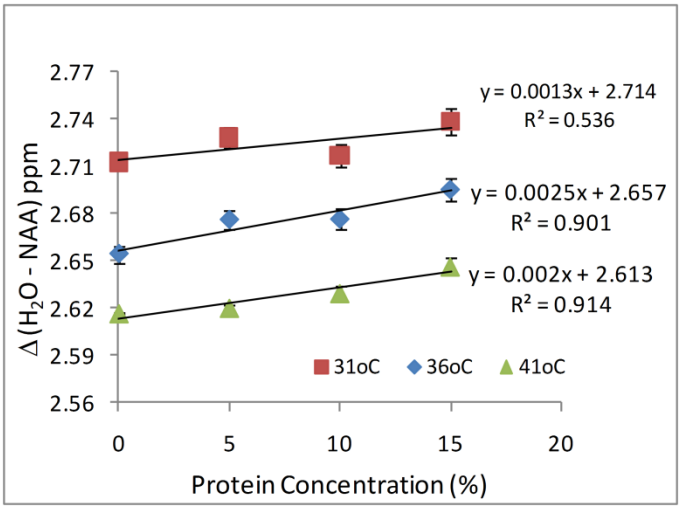
y = 0.0013x + 2.714
R² = 0.536
y = 0.0025x + 2.657
R² = 0.901
y = 0.002x + 2.613
R² = 0.914
31oC
36oC
41oC
Δ (H2O - NAA) ppm
Protein Concentration (%)

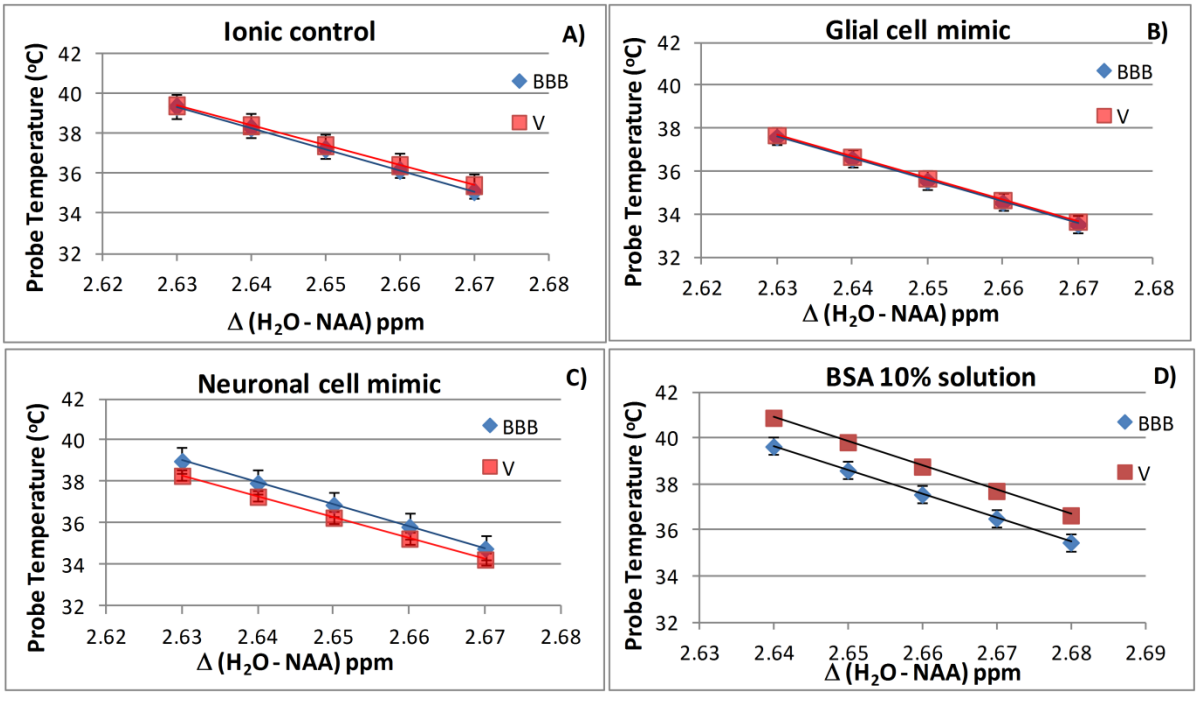
Ionic control
A)
Glial cell mimic
B)
Neuronal cell mimic
C)
BSA 10% solution
D)
BBB
V
Probe Temperature (ºC)
Δ (H2O - NAA) ppm